Article

pubs.acs.org/Biomac

Altering Peptide Fibrillization by Polymer Conjugation

Sabrina Dehn,[†] Valeria Castelletto,[‡] Ian W. Hamley,[‡] and Sébastien Perrier*[,†]

[†]Key Centre for Polymers and Colloids, School of Chemistry, The University of Sydney, NSW, 2006, Australia

[‡]Department of Chemistry, University of Reading, Whiteknights, Reading, RG6 6AD, United Kingdom

Supporting Information

ABSTRACT: A strategy is presented that exploits the ability of synthetic polymers of different nature to disturb the strong self-assembly capabilities of amyloid based β-sheet forming peptides. Following a convergent approach, the peptides of interest were synthesized via solid-phase peptide synthesis (SPPS) and the polymers via reversible addition−fragmentation chain transfer (RAFT) polymerization, followed by a copper(I) catalyzed azide−alkyne cycloaddition (CuAAC) to generate the desired peptide−polymer conjugates. This study focuses on a modified version of the core sequence of the β-amyloid peptide (Aβ), Aβ(16−20) (KLVFF). The influence of attaching short poly(*N*-isopropylacrylamide) and poly(hydroxyethylacrylate) to the peptide sequences on the self-assembly properties of the hybrid materials were studied via infrared spectroscopy, TEM, circular dichroism and SAXS. The findings indicate that attaching these polymers disturbs the strong self-assembly properties of the biomolecules to a certain degree and permits to influence the aggregation of the peptides based on their β-sheets forming abilities. This study presents an innovative route toward targeted and controlled assembly of amyloid-like fibers to drive the formation of polymeric nanomaterials.

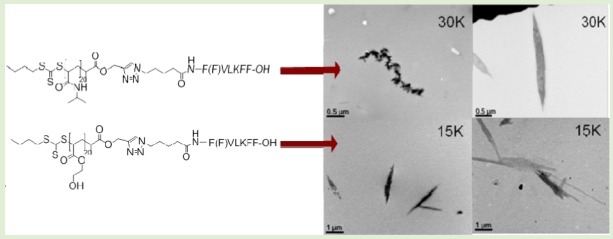

INTRODUCTION

Inspiration from nature and improved synthetic strategies have triggered dramatic advances in the development of multifunctional materials over the past two decades. The combination of biological materials such as proteins and peptides with synthetic polymers is of particular interest because the resultant conjugates benefit from the properties of both components.[1] These hybrid materials have found many diverse applications, such as tissue engineering,[2] drug delivery,[3] and structured nanomaterials.[4] Nanomaterials, in particular, benefit greatly from the self-organization properties of peptides, because they lead to hierarchical nanostructures of much higher complexity than those achievable with synthetic polymers.[5] For instance, nanostructures such as nanofibers[6] or nanotubes[7] based on self-assembled polypeptides can be applied in regenerative medicine[8] or nanoelectronics.[7] Various approaches to design peptide-based nanomaterials and how to control and trigger their self-assembly, have been described, including their use to guide the formation of supramolecular structures and related functionalities.[9,10] The challenge has now shifted to the incorporation of additional functional molecules such as polymers for the generation of highly functional nanostructured materials.[3,11] The self-organization properties of peptides or proteins can be used to encode structural information in the polymeric nanomaterials at the molecular level. In addition, the synthetic polymer section of these nanomaterials can also affect the self-organization properties of the peptides or proteins, thus changing their reactivity. Peptides and proteins are well-known to strongly self-assemble into β-sheets, which can further aggregate into ribbons and fibrils.[12] Indeed, β-sheet forming peptides have been intensively discussed in the past decade in the context of protein misfolding diseases,[13] such as Alzheimer's (AD)[14] and Parkinson's (PD) diseases.[15] In the case of AD, the β-amyloid peptide (Aβ) is believed to aggregate into fibrils and form amyloids,[16,17] and several studies suggest that a critical sequence for fibrillization is Aβ(16−20), KLVFF.[5,18] It has also recently been shown that addition of two more phenylalanine residues to that core sequence (FFKLVFF) permits even stronger aggregation via hydrophobic and aromatic interactions.[19] Recent work has focused on attaching synthetic polymers to these β-sheets forming peptide sequences to investigate the influence on the β-sheet forming properties.[4,20] Synthetic strategies for peptide/protein−polymer conjugates are well described,[3,11,21,22] and the properties of the peptide-polymer conjugates have been examined. For instance Pochan and co-workers used ethylene glycol modified amino acids to synthesize polypeptides that retain the α-helical structure of the amino acids.[23] In some cases, the self-assembly abilities of the conjugates and corresponding properties such as gel formation can be controlled by the degree of polymerization and the balance between α-helical and β-sheet structures.[24] Studies on the influence of conjugated synthetic polymeric chains to β-sheets forming peptides and their β-sheets forming properties in particular have also been reported.[4,25−28] For instance, Adams et al. have used polyethylene oxide (PEO) with side chain conjugated peptides to form vesicles,[29] and Tzokova et al. have demonstrated the importance of the nature of the peptide and

Received: May 8, 2012
Revised: July 8, 2012
Published: July 9, 2012

Scheme 1. (a) Solid Phase Supported Peptide Synthesis of N_3C_4−FVLKFF−OH (1) and N_3C_4−FFVLKFF−OH (2); (b) RAFT Polymerization To Yield $PNIPAAM_{20}$ (5) and $PHEA_{20}$ (6); (c) Microwave-Assisted CuAAC Reaction To Generate the FFVLKFF Conjugates 8 ($PNIPAAM_{20}$) and 10 ($PHEA_{20}$) and the FVLKFF Conjugates 7 ($PNIPAAM_{20}$) and 9 ($PHEA_{20}$)

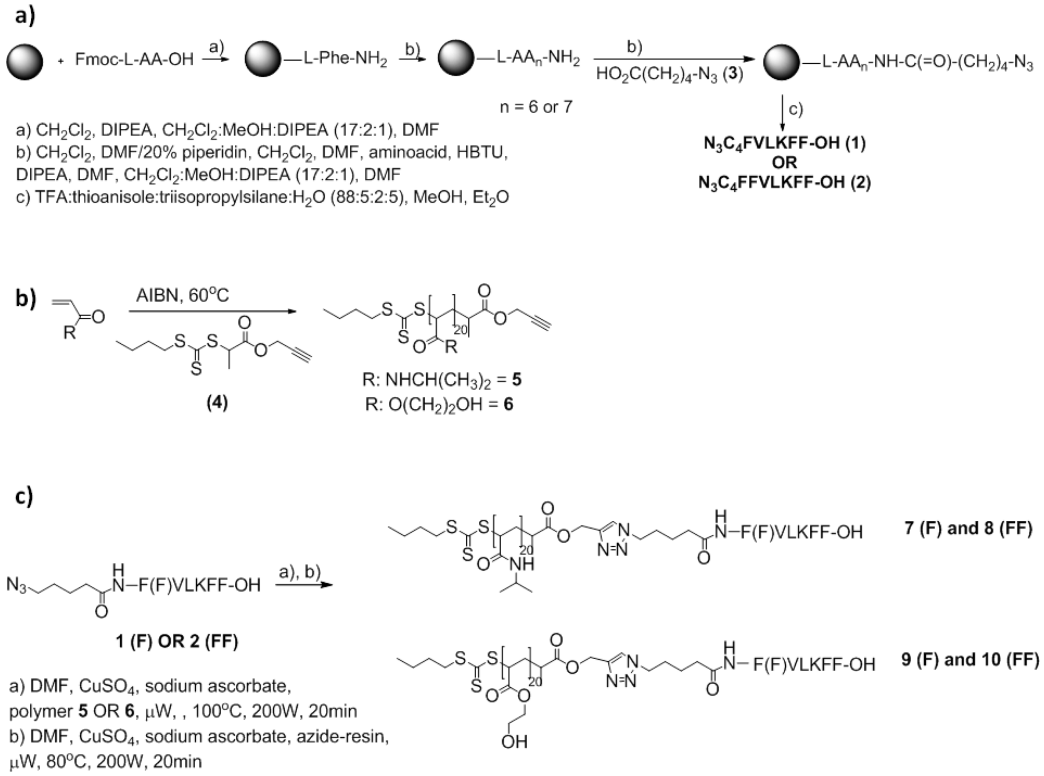

the relative balance between polymer and peptide for the self-assembly process.[30] However, there is limited precise investigation on the self-assembly properties of the resultant conjugates[4,27,31−36] and there is still a high demand on understanding this process to exploit the self-assembly properties with full capacity. Poly(ethylene glycol) (PEG) is the most common polymer used in research on peptide−polymer conjugates aggregation because it improves biocompatibility and decreases immunoresponse.[37] To date, PEG is the only polymer considered in studies involving the core sequence of the β-amyloid peptide (Aβ16−20),[20,25,31,38,39] and it has been reported that hydrophobically modified Aβ(16−20) sequences (FFKLVFF) form very strong self-assembled structures[19] that are retained even after PEGylation.[25] These initial results suggest that the nature of the peptide may dictate the suitability of a given conjugate polymer to alter the strong self-assembly properties of the β-sheet forming peptides. Herein, we describe a systematic investigation on the capability of a polar polymer (poly(hydroxylethyl acrylate), PHEA) and a less polar polymer (poly(*N*-isopropyl acrylamide), PNIPAAM) to influence the self-assembly properties of a β-sheet forming peptide. A modified Aβ(16−20) sequence with two additional phenylalanine units (FFVLKFF) was used as a model system. In addition, the Aβ(16−19) sequence, similarly modified with one phenylalanine units, (FVLKFF) was also investigated to assess the importance of phenylalanine in the peptide sequence. We opted for a convergent approach, in which the peptides and polymers were first synthesized via solid-phase peptide synthesis (SPPS) and reversible addition−fragmentation chain transfer (RAFT) polymerization respectively, followed by copper(I) catalyzed azide−alkyne cycloaddition (CuAAC) to generate the desired peptide-polymer conjugates (Scheme 1).

MATERIALS AND METHODS

Fmoc-Phe-OH, Fmoc-Lys(Boc)-OH, Fmoc-Leu-OH, Fmoc-Val-OH, 2-(1*H*-benzotriazole-1-yl)-1,1,3,3-tetramethyluronium (HBTU) were obtained from GL Biochem and used as supplied. Butyl-trithiocarbonate propanoicacid (BTCPA) was obtained from Dulux and used as supplied, and azoisobutyronitrile (AIBN) was obtained from Aldrich and precipitated from methanol prior to use. Hünig's base *N*,*N*-diisopropylethylamine (DIPEA), trifluoroacetic acid (TFA), thioansiol, triisopropylsilane, sulfurylchloride, and all solvents were ordered through Sigma-Aldrich and used as received. *N*-Isopropylacrylamide (NIPAAM) was purchased from Sigma-Aldrich and recrystallized before usage. Hydroxyethyl acrylate (HEA) was purchased from Sigma-Aldrich and was deinhibited before polymerization. All other chemicals were ordered through Sigma-Aldrich and used without any further purification.

Nuclear Magnetic Resonance (NMR). NMR analyses were carried out on Bruker Ultra Shield Avance Spectrometers (200 or 300 MHz). For all NMR analyses deuterated solvents as stated were used.

Size Exclusion Chromatography (SEC). SEC analyses were performed at 50 °C using a Agilent SEC system (PL-GPC50 Plus), equipped with a guard column and two Polar Gel-M columns (300 × 7.5 mm) and a PL-RI detector. The system was set at 32 °C with DMF using 0.1 wt % LiBr, 0.05 g/L hydroquinone with a flow rate of 0.7 mL/min. For sample analysis, a poly-styrene calibration has been used.

Transmission Electron Microscopy (TEM). Samples were prepared by placing a drop of sample solution on a carbon coated copper grid covered with thin film of pioloform. Samples were air-dried for at least 24 h before the analysis. TEM images were obtained using a JEOL1400 electron microscope.

Fourier Transform Infrared (FT-IR). FT-IR spectra were obtained using a Bruker ISF66v spectrometer FT-IR from dried film of sample solution. The numbers of scans were set at 32.

Electrospray Ionization Mass Spectroscopy. ESI analysis was performed using a Finnigan LCQ mass spectrometer.

Circular Dichroism Spectroscopy (CD). CD spectra were recorded using a Chirascan spectropolarimeter (Applied Photophysics, U.K.). Solutions of the peptides and conjugates in methanol were loaded in parallel plaque cells (Hellma quartz Suprasil), with a 0.1 or 1 mm path length. The CD data were measured using 1 s acquisition time per point and 0.5 nm step. The postacquisition smoothing tool from Chirascan software was used to remove random noise elements from the averaged spectra. A residual plot was generated for each curve in order to verify whether or not the spectrum has been distorted during the smoothing process. The CD signal from the methanol was subtracted from the CD data of the peptide solutions.

Small-Angle X-ray Scattering (SAXS). Experiments were performed on beamline ID02 at the ESRF, Grenoble, France. Samples, dissolved in methanol, were placed in a glass capillary mounted in a brass block for temperature control. Micropumping was used to minimize beam damage, by displacing a drop of the sample by 0.01−0.1 mm for each exposure. The sample-to-detector distance was 1.2 m, and the X-ray energy was 12.46 keV. The $q = 4\pi \sin \theta/\lambda$ (2θ is the scattering angle and λ is the wavelength) range was calibrated using silver behenate. Data processing (background subtraction, radial averaging) was performed using the software SAXSUtilities.

General Procedure for the Synthesis of Peptides 1 and 2. The azide modified peptides N_3C_4−FVLKFF (**1**) and N_3C_4−FFVLKFF (**2**) have been synthesized via standard solid-phase 9-fluorenylmethoxycarbonyl (Fmoc) peptide synthesis on a 2-chlorotrityl resin. A total of 2 g (1.5 mmol g^{-1}) 2-chlorotrityl resin was suspended in 5 mL DCM for 30 min in a fritted syringe (10 mL). After the solvent has been filtered off, a solution of Fmoc-L-phenylalanine−OH (6.0 mmol, 2.322 g) and *N*,*N*-diisopropylethylamine (DIPEA, Hünig's Base; 12 mmol, 3.08 g) in DMF (5 mL) was added and shaken for 2 h. The solvent was filtered off and the resin was washed with DCM/MeOH/DIPEA 17:2:1 (3 × 10 mL) to cap any unreacted peptide chains. After washing the resin with DCM (3 × 10 mL), DMF (3 × 10 mL), and DCM (3 × 10 mL), it was dried in vacuum to be used for further SPPS. UV−vis was used to determine a loading of 1.06 mmol Fmoc-L-phenylalanin−OH per g of resin. A total of 0.5 g resin was used for further SPPS. For coupling of each Fmoc-protected L-amino acid, the resin was swollen in 5 mL of DCM for 30 min and deprotected with 20% solution piperidin in DMF (2 × 5 mL) for 3 min. After washing the resin with DMF (3 × 10 mL), DCM (3 × 10 mL), and DMF (3 × 10 mL), a solution of Fmoc-L-amino acid−OH (1.5 equiv), HBTU (2 equiv) to activate the N-terminus, and DIPEA (5 equiv) in DMF (5 mL) was added and shaken overnight (16 h). The solvent was filtered off and the resin washed with DMF (5 × 10 mL) and unreacted chains capped with DCM/MeOH/DIPEA 17:2:1 (3 × 10 mL) for 2 × 3 min. After washing with DMF (5 × 10 mL), the next coupling step was performed. Upon addition of the last amino acid, the azide linker C_4N_3 **3**, was coupled under the same reaction conditions. A mixture of TFA/thioanisol/triisopropylsilane: H_2O = 88:5:2:5 (10 mL for 3 h) was used to isolate the desired peptide sequences **1** and **2** from the solid phase. The obtained solution was concentrated to near dryness, dissolved in a small amount of MeOH and precipitated from ice-cold Et_2O. If necessary, preparative HPLC (ACN, H_2O, TFA) was performed for purification. Drying in vacuum yielded the opaque solids **1** and **2** (0.127 g, 41%).

Analysis of ***1****.* ^{1}H NMR (d-TFA, 300 MHz) δ = 7.223−7.393 (m, 15H, H_{ar}), 6.860 (s, br, NH, NH_2), 4.994−5.060 (d, 3H, 19.8 Hz, C*H*NH backbone), 4.668−4.745 (d, J = 23.1 Hz, 2H, C*H*NH backbone), 4.467 (s, br, 1H, C*H*NH backbone), 3.442 (s, br, 2H, CH_2N_3), 3.176−3.324 (d, br, J = 44.4 Hz, 6H, CH_2Phe), 2.597 (s, br, 2H, CH_2NH_2), 2.144−2.212 (m, 3H, $COCH_2$-, $CH(CH_3)_2CH$), 1.379−2.024 (m, br, 13H, $CH_2CH_2N_3$, $CH_2CH_2CH_2N_3$, $CH_2CH_2CH_2NH_2$, $CH_2CH_2NH_2$, $CH_2(CH_2)_3NH_2$, $CH_2(CH(CH_3)_2)$, $CH(CH_3)_2CH_2$), 1.056−1.119 (m, br, 12H, CH_3 peptide side chains) ppm.

^{13}C NMR (d-TFA, 400 MHz) δ = 178 (COOH), 177 (NHCO−), 175 (NHCO−), 136 (C_{ar}-CH_2), 131 (C_{ar}, C_{ar}-CH_2), 129 (C_{ar}-CH_2), 120 (C_{ar}), 118 (C_{ar}), 116 (C_{ar}), 113 (C_{ar}), 19.5−62.5 (CH_3, CH_2, CH, 24C) ppm. MS (ESI$^+$) m/z = 925.25 (M+H$^+$, 100). IR (ATR FT-IR) ν = 3282 (m, NH-H), 2153 (w, N_3), 1679 (s, C═O, amide I), 1631 (m, C═O, amide I) cm^{-1}. HighRes MS found, 1072.59785 (M + H$^+$); calcd, 1071.59.

Analysis of ***2****.* ^{1}H NMR (d-TFA, 300 MHz) δ = 7.143−7.280 (m, 20H, H_{ar}), 6.775 (s, br, NH, NH_2), 4.933−4.977 (d, J = 13.2 Hz, 4H, C*H*NH backbone), 4.574−4.666 (d, J = 27.6 Hz, 2H, C*H*NH backbone), 4.322 (s, br, 1H, C*H*NH backbone), 3.077−3.359 (m, 10H, CH_2N_3, 14H, CH_2Phe), 2.490 (s, br, 2H, CH_2NH_2), 1.441−1.837 (m, 16H, *CH*, CH_2), 0.862−1.031 (m, 12H, CH_3 peptide side chains) ppm. ^{13}C NMR (d-TFA, 300 MHz) δ = 181.05 (COOH), 178.54 (NHCO−), 176.12 (NHCO−), 175.43 (NHCO−), 175.12 (NHCO−), 136.57 (C_{ar}-CH_2), 131.20 (C_{ar}, C_{ar}-CH_2), 129.92 (C_{ar}-CH_2), 120.15 (C_{ar}), 118.62 (C_{ar}), 115.07 (C_{ar}), 112.36 (C_{ar}), 18−62.27 (CH_3, CH_2, CH, 26C) ppm. MS (ESI$^+$) m/z = 1072.80 (M + H$^+$, 100). IR (ATR FT-IR) ν = 3420 (m, NH-H), 2113 (w, N_3), 1681 (s, C═O, amide I), 1629 (m, C═O, amide I) cm^{-1}. HighRes MS found, 925.52944 (M + H$^+$); calcd, 924.52.

Synthesis of 5-Azido Pentanoic Acid 3. The synthesis of the C_4N_3 linker followed a procedure from Srinivasan[40] and Kakwere.[33] Under inert conditions, bromovaleric acid (40 mmol, 7.24 g) was dissolved in 8 mL of MeOH and cooled down to 0 °C. Thionyl chloride (120 mmol, 14.27 g) was added dropwise under a N_2 atmosphere within 45 min and stirred for 30 min at 0 °C. The reaction mixture was allowed to warm up to room temperature and was stirred for 19 h. After solvent evaporation, the residue was suspended in 50 mL of ethyl acetate and extracted with $NaHCO_3$ (3 × 30 mL), H_2O (3 × 30 mL), and brine (1 × 30 mL). Drying over $NaSO_4$ and removing the solvent under reduced pressure lead to a brown liquid.

Upon addition of 30 mL of DMSO, NaN_3 (77 mmol, 5 g) was added under rapid stirring. This solution has been stirred at 50 °C for 24 h and the resultant white suspension has been taken up with 20 mL H_2O and was extracted with Et_2O (4 × 40 mL). Washing with brine, drying over $NaSO_4$ and removing the solvent under reduced pressure yielded in a brown oil. After dissolving in 30 mL of THF/H_2O = 3:1 (v/v), 20 mL of aqueous LiOH (73 mmol) was added and the mixture was stirred for 4 h at room temperature. THF was removed under reduced pressure and the aqueous phase was combined with 50 mL of ethyl acetate. Washing with 1 N HCl (3 × 50 mL), H_2O (3 × 50 mL), and brine (2 × 50 mL) and drying the combined organic phases over $NaSO_4$ and removing the solvent under reduced pressure yielded in **5** as brown oil (70.1%, 4.01 g).

^{1}H NMR ($CDCl_3$, 300 MHz) δ = 11.442 (s, 1H, OH), 3.233−3.276 (t, J = 12.9 MHz, 6.6 MHz, 2H, CH_2N_3), 2.328−2.375 (t, J = 14.1 MHz, 6.9 MHz, 2H, $CH_2(CH_2)_3N_3$), 1.547−1.726 (m, 4H, $CH_2CH_2N_3$) ppm. ^{1}H NMR data are in agreement with literature results.[33]

Synthesis of (Prop-2-ynyl propanoate)yl Butyltrithiocarbonate (PPBTC, 4). The alkyne-modified RAFT agent PPBTC **4** was synthesized as described by Konkolewicz et al.[41] Butyltrithiocarbonate propanoic acid (BTCPA; 2.06 g, 8.60 mmol) was dissolved in 50 mL DCM and cooled down to 0 °C. Propargyl alcohol (2.42 g, 23.02 mmol), EDCI (3.02 g, 12.62 mmol), and DMAP (0.13 g, 1.1 mmol) was added and stirred at 0 °C for 2 h. The reaction mixture was allowed to warm up to room temperature and was stirred for additional 16 h. Washing with H_2O (5 × 20 mL), drying over $MgSO_4$, and removing the solvents yielded a yellow oil. Purification was achieved via passing over a silica pad using toluene/ethyl acetate 9:1. Removing solvents and drying in vacuum gave the desired product **4** as yellow oil (91.7%, 2.16 g). ^{1}H NMR ($CDCl_3$, 300 MHz) δ = 4.802−4.876 (q, J = 7.5 Hz, 1H, $SCHCH_3CO$), 4.726 (t, J = 1.2 Hz, 2H, CH_2CCH), 3.30−3.379 (t, J = 7.2 Hz, 2H, $CH_3(CH_2)_2CH_2S$-), 2.482−2.498 (t, J = 2.4 Hz, 1H, CH_2CCH), 1.595−1.725 (m, 5H, $CH_3CH_2CH_2CH_2S$-, $SCHCH_3CO$), 1.385−1.484 (m, 2H, $CH_3CH_2(CH_2)_2S$-), 0.901−0.949 (t, J = 7.2 Hz, 3H, $CH_3(CH_2)_3S$-). Data are in agreement with results previously reported by Konkolewicz et al.[41]

General Procedure for the Synthesis of Polymers. The RAFT polymers were prepared according to a procedure previously reported by our group.[34,41,42] A mixture of monomer, removed from inhibitors, AIBN (AIBN/RAFT = 0.1:1 equiv) and solvents were added. The

Table 1. Synthetic Details and Characterization for Polymers

	polymer	[M]/ [RAFT]	time (h)	conversion[a] (%)	DP[a]	M_n[b]	$Đ$[b]
5	$PNIPAAM_{20}$	33:1	4	81	20	2540	5400
6	$PHEA_{20}$	33:1	3	88	23	2950	4600

[a]Determined via ^{1}H NMR spectroscopy. [b]Determined via SEC. SEC results uncorrected relative to PS standards.

Table 2. Microwave-Assisted Click Reaction between Azide Peptide and Alkyne Polymers

	molar equivalents						mL
	polymer		azide peptide		$CuSO_4{\cdot}5H_2O$	sodium ascorbate	DMF
7	$PNIPAAM_{20}$	1.2	N_3C_4-FVLKFF	1	2	10	5
8	$PNIPAAM_{20}$	1.2	N_3C_4-FFVLKFF	1	2	10	5
9	$PHEA_{20}$	1.2	N_3C_4-FVLKFF	1	2	10	5
10	$PHEA_{20}$	1.2	N_3C_4-FFVLKFF	1	2	10	5

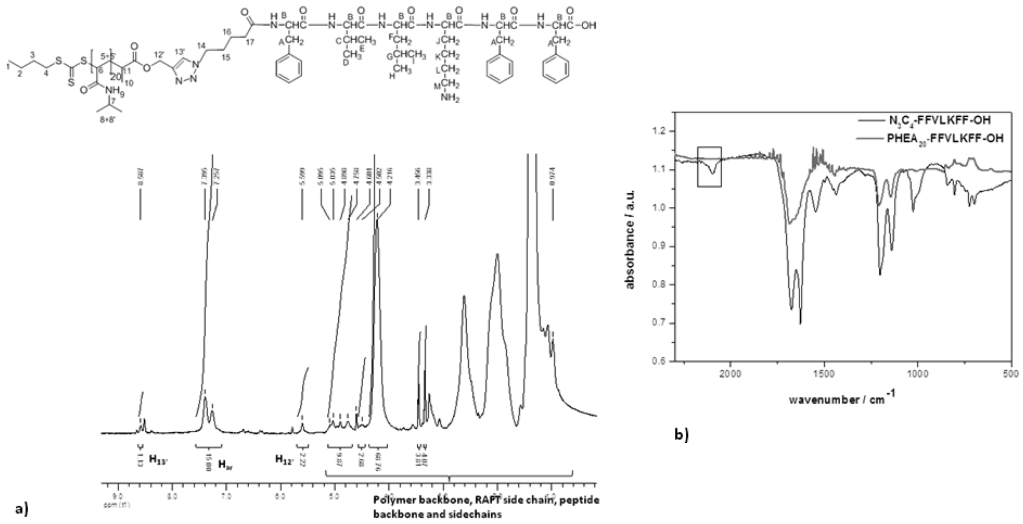

Figure 1. (a) ^{1}H NMR spectrum of $PNIPAAM_{20}$-FVLKFF conjugate **7** confirming the successful click reaction. (b) FT-IR spectrum from dried films of 1 wt % methanol solutions of $PHEA_{20}$-FFVLKFF conjugate **10**, showing the disappearance of the azide peak at 2153 cm^{-1} (black box) as a result of the successful click reaction.

reaction vessel was purged with N_2 for 15 min and left under a nitrogen atmosphere of 1 atm for the polymerization. *N*-isopropylacrylamide polymerization was performed in dioxane at 60 °C, hydroxyethyl acrylate in *tert*-butanol at 70 °C, and purified via precipitation from ice-cold hexane/Et_2O (4:1) or Et_2O. The molecular weight of the polymers were characterized by NMR and SEC.

*Analysis of **5** (Table 1).* ^{1}H NMR (d-TFA, 300 MHz) δ = 4.805 (s, 2H, CH_2, -O-CH_2-CCH), 4.142 (s, 22H, CH, -NH-$CH(CH_3)_2$), 3.460 (s, 2H, CH_2, CH_3-$(CH_2)_2$-CH_2-S-), 2.533, 2.378, 1.934, 1.769, 1.290–1.406 (polymer backbone, CH_3-CH_2-CH_2-CH_2-S-, -O-CH_2-CCH), 0.856–0.987 (m, 5H, CH_2, CH_3-CH_2-$(CH_2)_2$-S-, CH_3, CH_3-$(CH_2)_3$-S-) ppm.

*Analysis of **6** (Table 1).* ^{1}H NMR (DMSO-d_6, 300 MHz) δ = 4.769 (s, 23H, OH), 4.675 (s, 1H, −O−CH_2-CCH), 4.008 (s, 41H, -O-CH_2-CH_2-OH), 3.553 (s, 46H, -O-CH_2-CH_2-OH), 3.402 (s, 2H, CH_3-$(CH_2)_2$-CH_2-S-), 1.066–2.335 (m, polymer backbone, CH_3-CH_2-CH_2-CH_2-S-, CH_3-CH_2-CH_2-CH_2-S-), 0.863–0.901 (t, 3H, CH_3-$(CH_2)_3$-S-) ppm.

General Procedure for the Synthesis of Peptide–Polymer Conjugates 7–10. The azide peptide sequences **1** and **2** were combined with the correspondent alkyne polymers **5** and **6**, $CuSO_4{\cdot}5H_2O$, sodium ascorbate and 5 mL DMF. After vortex mixing, the reaction was carried out in a microwave reactor at 100 °C, 200 W, for 15 min under continuous stirring and N_2 cooling.

All four peptide polymer conjugates were purified by a second microwave-assisted click reaction at 80 °C using an azide resin to remove any unreacted polymers. The azide resin was synthesized according to procedure previously used in this group.[34] Excess of copper was removed via filtration through neutral alumina. The solvent was evaporated under reduced pressure; the resultant brown residue was washed with H_2O to remove any remains of sodium ascorbate. After centrifugation and drying in vacuum a brown solid could be isolated (64 mg, 43%).

The conjugates were characterized by using ^{1}H NMR. The disappearance of the peak for the alkyne proton and the methyl group next to the triple bond indicated a complete reaction of the alkyne polymer. In addition, ESI-MS has been used but none of the starting materials were detected, meaning peptide and polymer have been completely consumed by the click reaction. Furthermore the FT-IR spectra do not show any peaks correspondent to the azide, concluding that all azide has been completely reacted in the click reaction.

*Analysis of **7**.* ^{1}H NMR (d-TFA, 300 MHz) δ = 8.587 (s, 1H, $CCH_{triazole}$), 7.257–7.395 (d, br, 15H, H_{ar}), 5.599 (s, 2H, $OCH_2C_{triazole}$), 4.758–5.095 (m, 10H, OH polymer, CHNH backbone, NH), 0.974–4.502 (PNIPAAM backbone, RAFT side chain, peptide side chains) ppm.

*Analysis of **8**.* ^{1}H NMR (d-TFA, 300 MHz) δ = 8.385 (s, 1H, $CCH_{triazole}$), 7.347 (s, br, 20H, H_{ar}), 5.234 (s, 2H, $OCH_2C_{triazole}$), 1.045–4.993 (CHNH backbone, PNIPAAM backbone, RAFT side chain, peptide side chains) ppm.

*Analysis of **9**.* ^{1}H NMR (d-TFA, 300 MHz) δ = 8.902 (s, 1H, $CCH_{triazole}$), 7.646–7.778 (d, br, 15H, H_{ar}), 5.976 (s, 2H, $OCH_2C_{triazole}$), 1.046–5.203 (CHNH backbone, PNIPAAM backbone, RAFT side chain, peptide side chains) ppm.

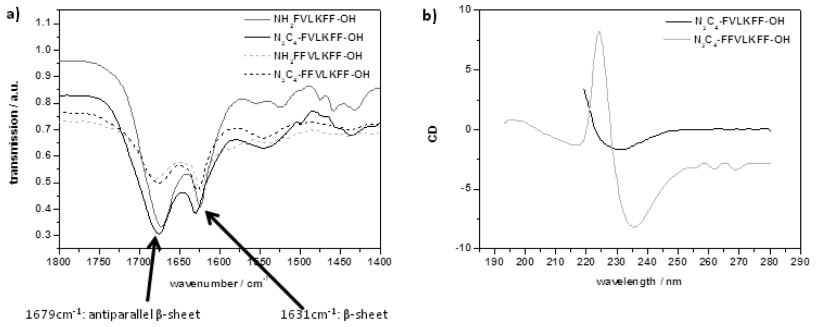

Figure 2. (a) FT-IR spectrum of amino peptides and correspondent azide modified peptides **1** and **2** displaying the characteristic bands for β-sheets around 1679 cm^{-1} and 1631 cm^{-1}. (b) Circular dichroism spectrum of azide peptides **1** and **2** showing the characteristic negative and positive bands for β-sheet structures.

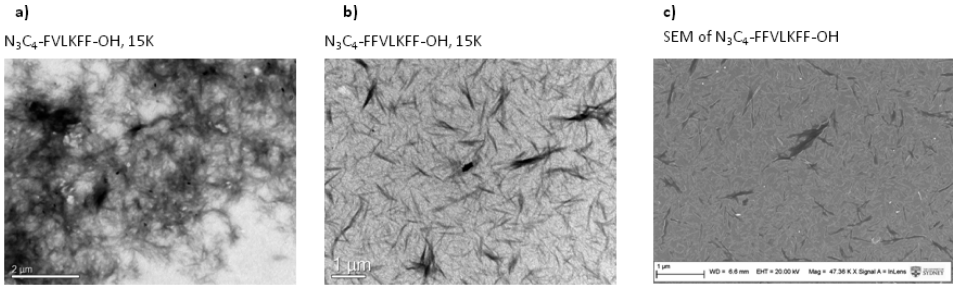

Figure 3. Typical TEM images of aggregates obtained from self-assembly of the conjugates (dried films of 1 wt % methanol solutions): (a) TEM image of N_3C_4–FVLKFF–OH **1**; (b) TEM image of N_3C_4–FFVLKFF–OH **2**; (c) SEM image of N_3C_4–FFVLKFF–OH **2**.

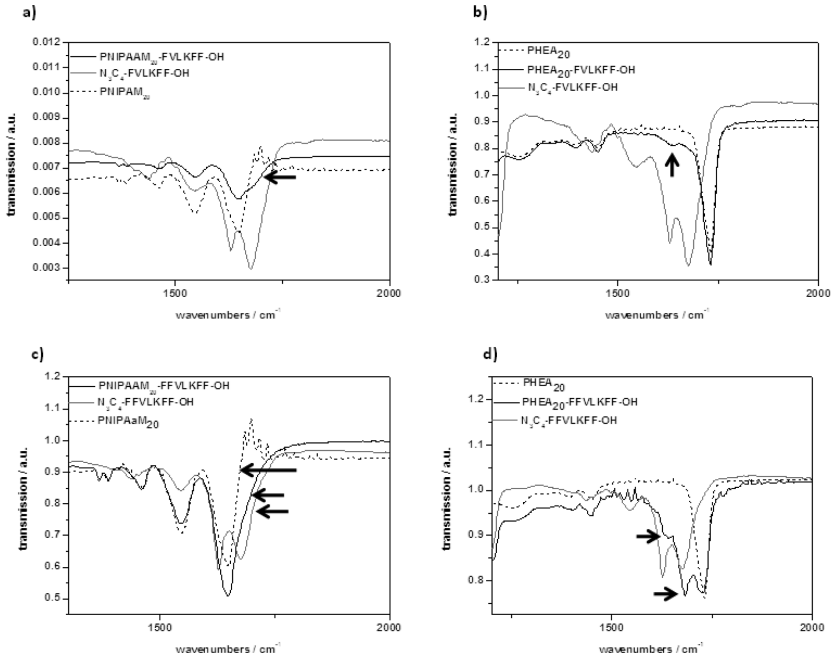

Figure 4. FT-IR spectra of conjugates **7** (a), **9** (b), **8** (c), and **10** (d) of dried films of 1 wt % methanol solutions. Arrows indicate the relevant bands or changes in band shapes.

Analysis of ***10****.* ^{1}H NMR (d-TFA, 300 MHz) δ = 8.614–8.690 (d, br, 1H, $CCH_{triazole}$), 7.341–7.486 (d, br, 20H, H_{ar}), 5.683 (s, 2H, $OCH_2C_{triazole}$), 0.501–5.131 (*CH*NH backbone, PNIPAAM backbone, RAFT side chain, peptide side chains) ppm.

■ RESULTS AND DISCUSSION

The azide and alkyne functionalities were introduced in the peptide and polymer segment, respectively, following procedures previously published by our group.[43] Azide-modified FVLKFF (**1**) and FFVLKFF (**2**) were synthesized via solid-phase peptide synthesis (SPPS), and the azide group was introduced at the N terminal. The polymers were synthesized via reversible addition–fragmentation chain transfer (RAFT) polymerization. The synthesis of the azide modified peptides **1** and **2** via SPPS leads to white solids in 41% yield (Scheme 1a), and were characterized by NMR spectroscopy, ESI-MS spectroscopy, high resolution mass spectrometry (High Res

dx.doi.org/10.1021/bm3007117 | *Biomacromolecules* 2012, 13, 2739–2747

Table 3. Amount (in Percentage) of Remaining β-Sheet Features in Conjugates 7−10

	β-sheet presence in samples	
	parallel	antiparallel
	1621−1639 cm^{-1}[a]	1660−1697 cm^{-1}[a]
	1614−1648 cm^{-1}[b]	1656−1708 cm^{-1}[b]
$PNIPAAM_{20}$-FVLKFF	26	10
$PNIPAAM_{20}$-FFVLKFF	17[c]	
$PHEA_{20}$-FVLKFF	8.5	24
$PHEA_{20}$-FFVLKFF	13	12

[a]Characteristic bands for parallel and antiparallel β-sheets found for FVLKFF-C_4N_3. [b]Characteristic bands for parallel and antiparallel β-sheets found for FFVLKFF-C_4N_3. [c]Conjugate **9** only displayed one broad band from overlapping bands of antiparallel and parallel β-sheet features.

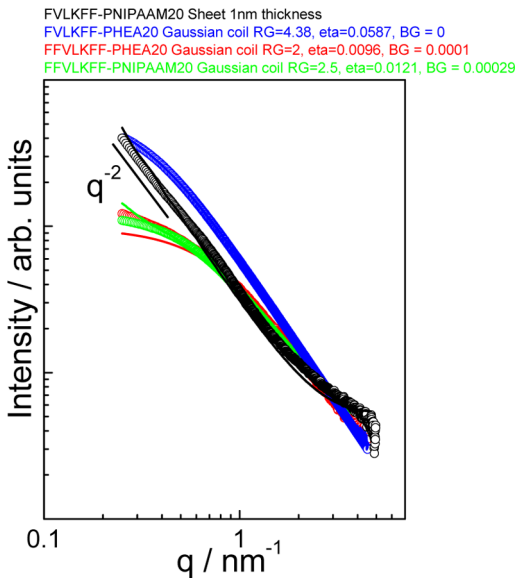

Figure 5. SAXS data for conjugates **7**−**10** (1 wt % in methanol) The solid line through the data for conjugate **7**−**10** is the model form factor fit for the Gaussian coil structure and the sheet-like structure, respectively, described in the text. (RG is the radius of gyration, eta is the contrast, BG is background.)

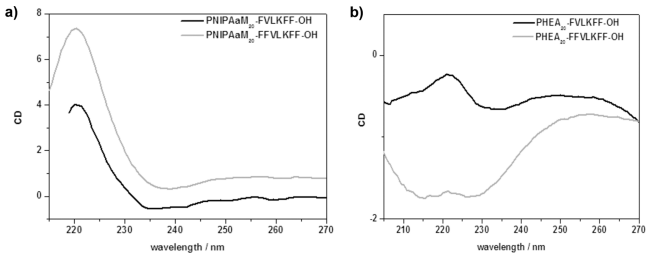

Figure 6. (a) Circular dichroism spectrum of $PNIPAAM_{20}$ conjugates **7** and **8** (1 wt % methanol); (b) circular dichroism spectrum of $PHEA_{20}$ conjugates **9** and **10** (1 wt % methanol).

MS), and Fourier transform infrared spectroscopy (FT-IR; SI). Polymerization of hydroxyethyl acrylate and *N*-isopropylacrylamide via reversible addition−fragmentation chain transfer (RAFT) polymerization[44−46] using chain transfer agent (CTA) **4** gave the functional polymers $PHEA_{20}$ **5** and $PNIPAAM_{20}$ **6** (Scheme 1b) with low polydispersities of 1.1 and 1.2, respectively (SI, Figure 5) and were verified via ^{1}H NMR

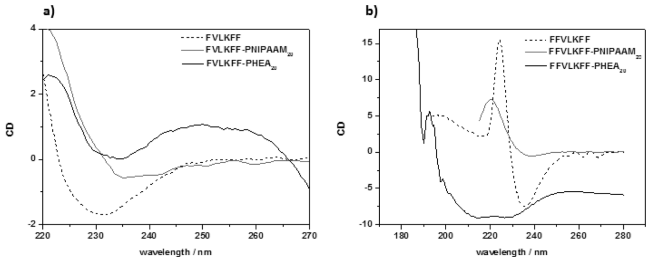

Figure 7. (a) Circular dichroism spectrum of FVLKFF **1** and correspondent $PNIPAAM_{20}$ and $PHEA_{20}$ conjugates **7** and **9** from 1 wt % methanol solution; (b) circular dichroism spectrum of FFVLKFF **2** and correspondent $PNIPAAM_{20}$ and $PHEA_{20}$ conjugates **8** and **10** from 1 wt % methanol solution.

(SI, Figure 6). The desired peptide−polymer conjugates **7**−**10** (Table 2) were synthesized via a convergent approach[42,47] using microwave-assisted copper-catalyzed azide−alkyne cycloaddition (CuAAC; Scheme 1c). Successful cycloaddition reaction was confirmed via ^{1}H NMR (Figure 1a; SI, Figures 7 and 8), FTIR (Figure 1b), and SEC (SI, Figure 9).

The ^{1}H NMR spectrum (Figure 1a) of $PNIPAAM_{20}$-FVLKFF conjugate **7** reveals the characteristic peak for the proton (H13′) at the newly triazole ring formed during the CuAAC at 8.587 ppm. The proton next to the ester functionality (H12) has been shifted downfield from 4.805 to 5.590 ppm (H12′), which confirms the successful coupling reaction. The disappearance of the azide band at 2153 cm^{-1} in the FT-IR spectrum (Figure 1b) of $PHEA_{20}$-FFVLKFF conjugate **10** verifies a successful conjugate formation. A shift of the SEC traces for $PNIPAAM_{20}$ and $PHEA_{20}$ indicates the successful coupling between the azide and alkyne. The SEC traces of the PNIPAAM conjugates **7** and **8** (SI, Figure 9) are shifted toward a longer retention time which indicates a higher hydrodynamic volume compared to the pure $PNIPAAM_{20}$. For both $PHEA_{20}$ conjugates **9** and **10**, the SEC traces are shifted to shorter retention times due to a lower hydrodynamic volume of the conjugates compared to the pure $PHEA_{20}$ (SI, Figure 9b).

Self-Assembly Studies. The self-assembly properties of peptides **1** and **2** and of the correspondent $PNIPAAM_{20}$ and $PHEA_{20}$ conjugates **7**−**10** have been studied in 1 wt % methanol solutions or as the related dried films of 1 or 5 wt % methanol solutions. FT-IR spectroscopy of dried films (1 wt % solutions in methanol) of **1** and **2** all show the characteristic bands for β-sheet assemblies at around 1631 cm^{-1} (parallel β-sheets) and 1679 cm^{-1} (antiparallel β-sheets),[48] indicating that the additional azide C_4-linker does not disturb the ability to form β-sheet assemblies (Figure 2a). Circular dichroism (CD) spectra of peptides **1** and **2** also reveal characteristic β-sheet features.[49] A negative band around 230 nm and a positive band at 218 nm is observed for **1** and a negative band at 235 nm and a positive band at 225 nm for **2** (Figure 2b).

The classical β-sheet circular dichroism spectrum has a minimum at 216−220 nm.[5,50] The red-shift for this minimum to 230 and 235 nm, respectively, is due to the formation of J-aggregates from a head-to-tail stacking of the aromatic units[51] and is a known feature for fiber formation.[49] These findings imply the presence of β-sheet structures in both azide peptides **1** and **2**. A strong band at 225 nm observed for **2**, which results from the fourth phenylalanine residue, shows the influence of these additional $\pi-\pi$ stacking interaction on the secondary structure of the peptide. Measurements using different concentrations display a concentration dependency of the

dx.doi.org/10.1021/bm3007117 | *Biomacromolecules* 2012, 13, 2739−2747

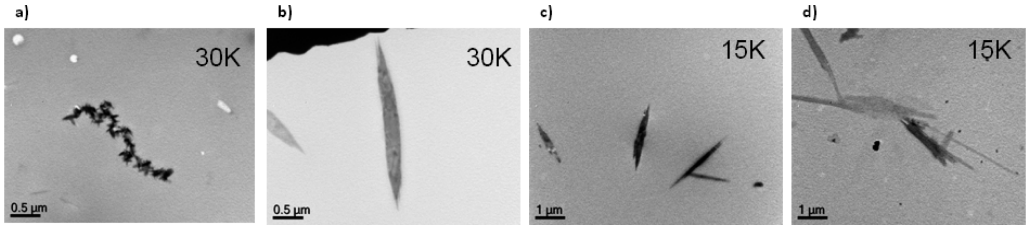

Figure 8. Typical TEM images of aggregates obtained from self-assembly of the conjugates (dried films of 1 wt % methanol solutions): (a) $PNIPAAM_{20}$-FVLKFF, (b) $PNIPAAM_{20}$-FFVLKFF, (c) $PHEA_{20}$-FVLKFF, and (d) $PHEA_{20}$-FFVLKFF conjugates. Magnification is displayed on the top right corner of each image.

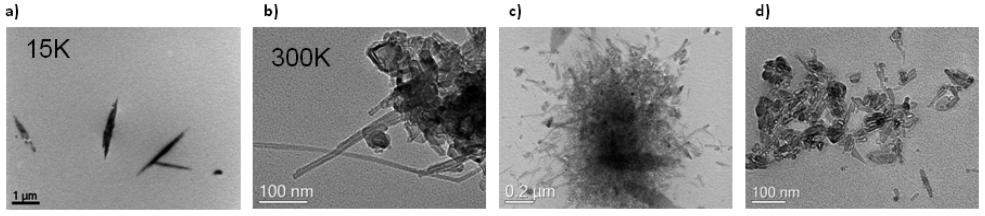

Figure 9. TEM images of self-assembled aggregates (dried films of 1 wt % methanol solution): (a) freshly prepared $PHEA_{20}$-FVLKFF-OH **9** (1 wt %); (b) incubated $PHEA_{20}$-FVLKFF-OH **9** (1 wt %); (c) incubated $PHEA_{20}$-FVLKFF-OH **9** (5 wt %); incubated $PHEA_{20}$-FFVLKFF-OH **10** (5 wt %).

formation of β-sheet structures. At low concentration (0.16 wt %), only a weak band around 230 nm could be observed, but upon increasing the concentration to 0.63 and 0.9 wt %, clear features for β-sheet structures could be obtained (SI, Figure 10). This observation confirms that the addition of the azide linker does not destroy the β-sheet forming abilities.

TEM and SEM images were obtained from dried films of 1 wt % methanol solutions on carbon coated copper TEM grids. One of the advantages of applying CuAAC to generate the desired conjugates is that no additional staining of the TEM samples is required.[42] The azide peptides **1** and **2** clearly show strong entangled networks (Figure 3), which points out the strong ability of **1** and **2** to not only form β-sheet assemblies as supported by FT-IR and CD data, but also to aggregate in larger structures.

The aggregation properties of the conjugates were investigated by FT-IR, CD, TEM, and SAXS. FT-IR spectra show that FFVLKFF conjugates **8** ($PNIPAAM_{20}$) and **10** ($PHEA_{20}$) and FVLKFF conjugates **7** ($PNIPAAM_{20}$) and **9** ($PHEA_{20}$) are still able to form β-sheet assemblies (Figure 4). The FT-IR spectrum of $PNIPAAM_{20}$-FVLKFF conjugates **7** displays a slight shoulder at 1691 cm^{-1} (Figure 4a, black arrow), which implies the presence of antiparallel β-sheets. The correspondent band around 1630 cm^{-1} from the parallel β-sheets is covered under the broad band from the PNIPAAM residue at 1652 cm^{-1}. We conclude that the broadness of the band for conjugate **7** around 1652 cm^{-1} and the appearance of the shoulder at 1691 cm^{-1} is evidence for the presence of β-sheet structures that overlap with the C═O stretching band of the PNIPAAM. The FT-IR spectrum of the $PNIPAAM_{20}$-FFVLKFF conjugate **9** (Figure 4b) shows a strong band around 1733 cm^{-1} resulting from the C═O stretching band from the ester group of the PHEA side chain. At 1637 and 1685 cm^{-1} appear two bands that are assigned to β-sheet structures (β-sheet and antiparallel β-sheet, respectively). From these results we conclude that the attachment of $PHEA_{20}$ does prevent the formation of strong fiber like networks but β-sheets are still formed. For $PNIPAAM_{20}$-FVLKFF conjugate **8**, two bands at 1550 and 1652 cm^{-1} (Figure 4c) were observed resulting from the PNIPAAM residues and no shoulder around 1691 $cm^{-1}$was observed. However, since the broadness of the band at 1652 cm^{-1} for **8** is much more pronounced than the band for the pure PNIPAAM (Figure 4c, indicated with arrows). We conclude that the C═O stretching band from PNIPAAM overlay the bands from parallel and antiparallel β-sheets. Further proof for the existence of β-sheet structures is discussed below. The FT-IR spectrum of the $PNIPAAM_{20}$-FFVLKFF conjugate **10** shows also a strong band around 1733 cm^{-1} from the ester group of the PHEA side chain. In addition, bands at 1687 and 1644 cm^{-1} are observed (Figure 4d, marked with arrows), which are assigned to antiparallel and parallel β-sheets, respectively.

FTIR second derivatives (sav-Golay) was used to determine the remaining amount of antiparallel and parallel β-sheets in the four conjugates. The desired bands of the second derivatives of the FTIR spectrum were integrated and compared to the correspondent integrals of the peptides N_3C_4−FVLKFF−OH **1** (1660−1697 cm^{-1}, parallel) and N_3C_4−FFVLKFF−OH **2** (1621−1639 cm^{-1}, antiparallel; Table 3). We find the amount of β-sheet features has been reduced from 100% in the pure peptides **1** and **2** to values between 10 and 25%. Interestingly, the nature of the conjugate seems to affect the type of β-sheet assembly observed for the FVLKFF-based conjugate, varying from a majority of parallel when conjugated to $PNIPAAM_{20}$ to antiparallel when conjugated to $PHEA_{20}$. In the case of FFKLVFF, the mixture of both types is kept, although peak overlap did not allow for differentiation between parallel and antiparallel β-sheet in the case of $PNIPAAM_{20}$-FVLKFF.

To investigate whether the FT-IR features are due to the conjugates **7**−**10**, FT-IR mixing experiments were performed using peptides **1** and **2** and $PNIPAAM_{20}$ and $PHEA_{20}$ in a 1:1 mixture (SI, Figures 11 and 12). For all four conjugates, a clear red-shift of the amide bands is obtained, which is indicative of the formation of sheet-like aggregates. Moreover, the mixture of FVLKFF **1** and $PNIPAAM_{20}$ **5** displays a distinct shoulder in the related amide band around 1650 cm^{-1}, indicating the presence of two different species in the solution with overlapping FT-IR bands. The FT-IR spectrum of the mixing

dx.doi.org/10.1021/bm3007117 | *Biomacromolecules* 2012, 13, 2739−2747

experiment with FFVLKFF **2** and $PNIPAAM_{20}$ **5** in a 1:1 mixture (SI, Figure 11b) shows a splitting of the band at 1652 cm^{-1} that is associated with the presence of two discrete compounds.

SAXS measurements on the FFVLKFF conjugates **8** ($PNIPAAM_{20}$) and **10** ($PHEA_{20}$) and on the FVLKFF conjugates **7** ($PNIPAAM_{20}$) and **9** ($PHEA_{20}$) in methanol (1 wt %) do not show any aggregation for conjugates **8**−**10** under the conditions modeled by SAXS (Figure 5). In fact, the SAXS data for conjugates **8** ($PNIPAAM_{20}$) and **10** ($PHEA_{20}$) can be modeled as Gaussian coils with a radius of gyration 2−2.5 nm, which is reasonable considering the polymer chain dimensions. For the FVLKFF conjugate **9**, it was also possible to fit the data to a Gaussian coil model. However, the obtained radius of gyration (4.4 nm) is larger than for the FFVLKFF conjugates. Gaussian coil form factor fitting was less successful for the SAXS data for conjugate **7** because the SAXS intensity exhibits an extended range (including low q) with a q^{-2} dependence. This indicates aggregation, consistent with the TEM images, and this intensity scaling is in fact expected for a sheet-like structure. Therefore, the SAXS data for conjugate **7** was fitted to a model of a homogeneous sheet (i.e., a planar object with extended lateral dimensions but finite thickness and a uniform electron density) of thickness 1 nm (30% thickness polydispersity). This demonstrates that the polarity of the conjugate, mostly dictated by the polymer block, and the polarity of the solvent used for the aggregation studies direct the "nature" of the conjugates in solution. These somewhat surprising results from SAXS analysis could be attributed to a concentration effect and the state of the equilibrium of the self-assembly process.

Circular dichroism was used as an additional technique to verify the FTIR and SAXS data. Spectra were obtained from 1 wt % solutions of the conjugates in methanol. The CD spectra of $PNIPAAM_{20}$ conjugates **7** and **8** and $PHEA_{20}$ conjugates **9** and **10** (Figure 6a and 6b) in methanol display bands for β-sheet assemblies and confirm the FT-IR results. $PNIPAAM_{20}$ conjugates **7** and **8** display a negative maximum at 235 nm and a positive maximum at 220 nm (Figure 2a). The corresponding $PHEA_{20}$ conjugate **9** displays a minimum at 235 nm and a dominating maximum at 225 nm, confirming the presence of β-sheets and aromatic stacking (Figure 6b). For conjugate **10**, a broad minimum around 215−230 nm is observed as a result of a strong β-sheet component and a small band at 225 nm for the $\pi\pi$-stacking from the aromatic residues (Figure 6b). The observed red-shift of the minimum around 218 to 230 nm in all four spectra are induced by strong maximum from the $n-\pi^*$ aromatic interactions.[52]

The CD spectra also support the conclusion by SAXS experiments that the peptide aggregation is disturbed by $PNIPAAM_{20}$ and $PHEA_{20}$. Indeed, FVLKFF conjugate **7** ($PNIPAAM_{20}$) shows a red shift of the negative band from 230 to 235 nm and PHEA-FFVLKFF **10** displays a blue shift and an intensive broadening of the band.

The CD spectrum of FFVLKFF conjugate **8** shows similar bands to the unconjugated peptide, indicating that the additional fourth phenylalanine residue strengthens the self-assembled structure, despite the presence of PNIPAAM. CD spectra of the PHEA conjugates **9** and **10** (Figure 7a,b) show typical β-sheet bands with a maximum at 195 nm and a minimum at 218 nm. We rationalize these observations by the ability of the polymer chain to alter the aggregation of the peptide segment depending on the nature of the polymer conjugate. PNIPAAM chains interact with the peptide segment, possibly as it is less favored by the solvent (methanol) and via H-bond formation between the amide groups found in the peptide and the acrylamide repeating units. Such interactions do not completely prevent β-sheet assemblies, but strongly disturb aggregation in larger structures. The introduction of a fourth phenylalanine residue in the peptide segment strengthens the peptide assemblies and allows for the formation of larger aggregates, despite the presence of the PNIPAAM chain. The more polar PHEA chains have greater interactions with the solvent and do not affect to the same extent β-sheet formation. The PHEA conjugate only partially prevents aggregation and favors dispersion in the solvent, thus, leading to the formation of smaller structures. We have previously observed that conjugating PHEA to the β-sheet forming peptide P_{11}-2 prevents the assembly of the peptidic segment.[33] This highlights the much stronger tendency of peptides **1** and **2** compared to peptide P_{11}-2 to aggregate into β-sheet-like structures and the importance of the functionality of the polymer to interfere with the peptide fibrillization.

TEM images of all four conjugates (Figure 8) reveal a small number of large aggregates and confirm that attaching the polymers to peptides **1** and **2**, although not extensively disturbing β-sheet formation, prevents the formation of strongly entangled networks.

TEM also confirmed that the self-assembly process of the conjugates into sheet-like aggregates is time- and concentration-dependent, an observation also made by CD spectroscopy. Indeed, TEM images from freshly prepared conjugate solutions (1 wt % in methanol) show only small and thin aggregates (Figure 9a; SI, Figures 13 and 14, left). However, allowing the aggregates to self-assemble for 66 h lead to an increased length (∼50−200 nm) and diameter (∼10−20 nm) in the range expected for amyloidal structures[52] (Figure 9b; SI, Figures 13 and 14, right), indicating that the peptide part of the conjugate still has an impact on the overall properties of the conjugate and that the peptide properties become more pronounced after a period of time. However, even after 66 h of incubation of the self-assembly process the entanglement of the aggregates are much less compared to the peptides **1** and **2** themselves. Increasing the concentration from 1 to 5 wt % in $PHEA_{20}$ conjugates **9** (Figure 9c) and **10** (Figure 9d) led to the formation of larger and more structured aggregates.

CONCLUSION

In conclusion, we have described a synthetic strategy and self-assembly studies for novel peptide−polymer conjugates, utilizing the manipulation of the self-assembly process via modified sequences from the β-amyloid peptide. Attaching short polymers of different functionality, $PNIPAAM_{20}$ and $PHEA_{20}$, to these peptide sequences disturbs their strong fibrillization properties and offers some degree of control over their aggregation. FTIR and circular dichroism measurements display some β-sheet features in the peptide−polymer conjugates **7**−**10**. However, second derivative calculations of the FTIR data confirm that conjugating $PNIPAAM_{20}$ or $PHEA_{20}$ to the peptides **1** and **2** reduces the amount of β-sheet features in the conjugate up to 80%. Models from SAXS experiments displayed sheet like structures for FVLKFF conjugates **7** ($PNIPAAM_{20}$) and coil-like structures for the other three conjugates, most likely due to concentration and polarity effects of the conjugate and the solvent. Overall our findings point out that a sensible choice in the nature of the

polymer conjugate in relation to the solvent may allow control over the self-assembly process. This approach is a promising way to address the challenging task to control the strong aggregation of β-sheet forming peptides and their use for controlled synthesis of functionalized supramolecular polymeric structures.

■ ASSOCIATED CONTENT

Supporting Information

NMR, ESI, high resolution mass spectrometry (High Res MS), Fourier transform infrared spectroscopy (FTIR), size exclusion chromatography (SEC), transmission electron microscopy (TEM), and circular dichroism (CD). This material is available free of charge via the Internet at http://pubs.acs.org.

■ AUTHOR INFORMATION

Corresponding Author

*Tel.: +61 (2) 9351 3366. Fax: +61 (2) 9351 3329. E-mail: sebastien.perrier@sydney.edu.au.

Notes

The authors declare no competing financial interest.

■ ACKNOWLEDGMENTS

The ARC (Discovery Program DP1096651) and the EPSRC (EP/F048114/1, EP/G026203/1, and EP/G067538/1) is gratefully acknowledged for financial support. The authors thank Ashkan Dehsorkhi for assistance with the CD measurements and Dr. Elizabeth Carter for support with the FTIR data fitting.

■ REFERENCES

(1) Klok, H.-A. *J. Polym. Sci., Part A* **2005**, *43*, 1−17.
(2) Drotleff, S.; Lungwitz, U.; Breunig, M.; Dennis, A.; Blunk, T.; Tessmar, J.; Göpferich, A. *Eur. J. Pharm. Biopharm.* **2004**, *58*, 385−407.
(3) Klok, H.-A. *Macromolecules* **2009**, *42*, 7990−8000.
(4) Rösler, A.; Klok, H. -A.; Hamley, I. W.; Castelletto, V.; Mykhaylyk, O. O. *Biomacromolecules* **2003**, *4*, 859−863.
(5) Hamley, I. W. *Angew. Chem., Int. Ed.* **2007**, *46*, 8128−8147.
(6) Hartgerink, J. D.; Beniash, E.; Stupp, S. I. *Science* **2001**, *294*, 1684−1688.
(7) Reches, M.; Gazit, E. *Science* **2003**, *300*, 625−627.
(8) Yang, Y. L.; Khoe, U.; Wang, X. M.; Horii, A.; Yokoi, H.; Zhang, S. G. *Nano Today* **2009**, *4*, 193−210.
(9) Ulijn, R. V.; Smith, A. M. *Chem. Soc. Rev.* **2007**, *37*, 664−675.
(10) Zelzer, M.; Ulijn, R. V. *Chem. Soc. Rev.* **2010**, *39*, 3351−3357.
(11) Gauthier, M. A.; Klok, H. -A. *Chem. Commun.* **2008**, 2591−2611.
(12) Aggeli, A.; Bell, M.; Boden, N.; Keen, J. N.; Knowles, P. F.; McLeish, T. C. B.; Pitkeathly, M.; Radford, S. E. *Nature* **1997**, *386*, 259−262.
(13) Dobson, C. M. *Nature* **2003**, *426*, 884.
(14) Goedert, M.; Spillantini, M. G. *Science* **2006**, *314*, 777.
(15) McLean, P. J.; Kawamata, H.; Hyman, B. T. *Neuroscience* **2001**, *104*, 901−912.
(16) Kahn, S. E.; Andrikopoulos, S.; Verchere, C. B. *Diabetes* **1999**, *48*, 241−253.
(17) Chimon, S.; Shaibat, M. A.; Jones, C. R.; Calero, D. C.; Aizezi, B.; Ishii, Y. *Nat. Struct. Mol. Biol.* **2007**, *14* (12), 1157−1164.
(18) Tjernberg, L. O.; Lilliehook, C.; Callaway, D. J. E.; Naslund, J.; Hahne, S.; J., T.; Terenius, L.; Nordtsedt, C. *J. Biol. Chem.* **1997**, *272*, 12601.
(19) Krysmann, M. J.; Castelletto, V.; Hamley, I. W. *Soft Matter* **2007**, *3*, 1401−1406.
(20) Krysmann, M. J.; Castelletto, V.; Kelarakis, A.; Hamley, I. W.; Hule, R. A.; Pochan, D. J. *Biochemistry* **2008**, *47*, 4597−4605.
(21) Dehn, S.; Chapman, R.; Jolliffe, K.; Perrier, S. *Polym. Rev.* **2011**, *51*, 214−234.
(22) Canalle, L. A.; Loewik, D. W. P. M.; Van Hest, J. C. M. *Chem. Soc. Rev.* **2010**, *39*, 329−353.
(23) Yu, M.; Nowak, A. P.; Deming, T. J.; Pochan, D. J. *J. Am. Chem. Soc.* **1999**, *121*, 12210−12211.
(24) Kotharangannagari, V. K.; Sánchez-Ferrer, A.; Ruokolainen, J.; Mezzenga, R. *Macromolecules* **2012**, *45*, 1982−1990.
(25) Hamley, I. W.; Krysmann, M. J. *Langmuir* **2008**, *24*, 8210−8214.
(26) Johnson, J. C.; Wanasekara, N. D.; Korley, L. T. J. *Biomacromolecules* **2012**, *13*, 1279−1286.
(27) Radu, L. C.; Yang, J.; Kopecek, J. *Macromol. Biosci.* **2009**, *9*, 36−44.
(28) Shaytan, A. K.; Schillinger, E.-K.; Khalatur, P. G.; Mena-Osteritz, E.; Hentschel, J.; Börner, H. G.; Bäuerle, P.; Khokhlov, A. R. *ACS Nano* **2011**, *5* (9), 6894−6909.
(29) Adams, D. J.; Atkins, D.; Cooper, A. I.; Furzeland, S.; Trewin, A.; Young, I. *Biomacromolecules* **2008**, *9*, 2997−3003.
(30) Tzokova, N.; Fernyhough, C. M.; Butler, M. F.; Armes, S. P.; Ryan, A. J.; Topham, P. D.; Adams, D. J. *Langmuir* **2009**, *25* (18), 11082−11089.
(31) Burkoth, T. S.; Benzinger, T. L. S.; Jones, D. N. M.; Hallenga, K.; Meredith, S. C.; Lynn, D. G. *J. Am. Chem. Soc.* **1998**, *120*, 7655−7656.
(32) Rathore, O.; Winningham, M. J.; Sogah, D. Y. *J. Polym. Sci., Part A* **2000**, *38*, 352−366.
(33) Kakwere, H.; Payne, R. J.; Jolliffe, K. A.; Perrier, S. *Soft Matter* **2011**, *7*, 3754−3757.
(34) Chapman, R.; Jolliffe, K.; Perrier, S. *Polym. Chem.* **2011**, *2*, 7977−7979.
(35) Hentschel, J.; Börner, H. G. *Macromol. Biosci.* **2009**, *9*, 187−194.
(36) Börner, H. G. *Prog. Polym. Sci.* **2009**, *34*, 811−851.
(37) Harris, J. M.; Chess, R. B. *Nat. Rev. Drug Discovery* **2003**, *2*, 214−221.
(38) Castelletto, V.; Newby, G. E.; Zhu, Z.; Hamley, I. W. *Langmuir* **2010**, *26* (12), 9986−9996.
(39) Burkoth, T. S.; Benzinger, T. L. S.; Urban, V.; Lynn, D. G.; Meredith, S. C.; Thiyagarjan, P. *J. Am. Chem. Soc.* **1999**, *121*, 7429−7430.
(40) Srinivasan, R.; Tan, L. P.; Wu, H.; Yang, P. Y.; Kalesh, K. A.; Yao, S. Q. *Org. Biomol. Chem.* **2009**, *7* (9), 1821−1828.
(41) Konkolewicz, D.; Gray-Weale, A.; Perrier, S. *J. Am. Chem. Soc.* **2009**, *131*, 19075−19077.
(42) Zhao, Y.; Perrier, S. *Chem. Commun.* **2007**, *41*, 4294−4296.
(43) Poon, C. K.; Chapman, R.; Jolliffe, K. A.; Perrier, S. *Polym. Chem.* **2012**, *3*, 1820−1826.
(44) Moad, G.; Rizzardo, E.; Thang, S. H. *Aust. J. Chem.* **2009**, *62*, 1402−1472.
(45) Perrier, S.; Takolpuckdee, P. *J. Polym. Sci., Part A* **2005**, *43*, 5347−5493.
(46) Semsarilar, M.; Perrier, S. *Nat. Chem.* **2010**, *2*, 811−820.
(47) Kakwere, H.; Chun, C. K. Y.; Jolliffe, K. A.; Payne, R. J.; Perrier, S. *Chem. Commun.* **2010**, *46*, 2188−2190.
(48) Haris, P.; Chapman, D. *Biopolymers* **1995**, *37*, 251−263.
(49) Hamley, I. W.; Nutt, D. R.; Brown, G. D.; Miravet, J. F.; Escuder, B.; Rodriguez-Liansola, F. *J. Phys. Chem. B* **2010**, *114* (2), 940−951.
(50) Kelly, S. M.; Jess, T. J.; Price, N. C. *Biochim. Biophys. Acta* **2005**, *1751*, 119−139.
(51) Whitten, D. G. *Acc. Chem. Res.* **1993**, *26*, 502−509.
(52) Castelletto, V.; Hamley, I. W.; Harris, P. J. F. *Biophys. Chem.* **2008**, *138*, 29−35.